Acta Oceanol. Sin., 2024, Vol. 43, No. 12, P. 1–12
https://doi.org/10.1007/s13131-024-2365-0
http://www.aosocean.com
E-mail: ocean2@hyxb.org.cn

Intercomparison of conventional and new methods for estimating eddy kinetic energy

Wenyu Li[1], Guidi Zhou[1, 2*], Xuhua Cheng[1]

[1] College of Oceanography, Hohai University, Nanjing 210098, China

[2] Key Laboratory of Marine Hazards Forecasting of Ministry of Natural Resources, Hohai University, Nanjing 210098, China

Received 29 February 2024; accepted 9 July 2024

Abstract

We introduce a new method, the piecewise Reynolds mean (PREM), for decomposing the flow velocity into the mean-flow and eddy-flow parts in the time domain for subsequent calculation of the mean flow kinetic energy (MKE) and eddy kinetic energy (EKE). Compared with conventional methods like the Reynolds mean and running mean (RUM), PREM has the advantage of exact balance between the MKE and EKE, without the additional residual kinetic energy (RKE), while retaining time-dependent mean-flow. It is mathematically simple and computationally lightweight, depending on a pre-defined separation scale for the mean-flow and eddies. Based on satellite observations and the separation scale of 1 year, we compare PREM with RUM, as well as another newly proposed method, the eddy detection and extraction (EDEX). The latter is based on objective identification of mesoscale eddies and eddy anomaly extraction algorithms, and is therefore only suitable for mesoscale eddy energetics, but independent of separation scales. It is shown that compared with RUM, PREM gives larger mean EKE and stronger interannual variability. In strong-current and eddy-rich regions, the two methods differ the most (max: Kuroshio Extension, root-mean-sqaure-difference = 60.3 J/m^3); but in areas with weak current and eddy, the difference accounts for the largest fraction of total EKE (max: south of the Aleutian Islands, 208%). EKE estimated by the two methods is out of phase (min correlation coefficient = 0.38). The mean EKE and standard deviation from the EDEX method resemble the PREM with 1-year separation scale, but is generally smaller in magnitude.

Key words: mesoscale eddy, kinetic energy, piecewise Reynolds mean

Citation: Li Wenyu, Zhou Guidi, Cheng Xuhua. 2024. Intercomparison of conventional and new methods for estimating eddy kinetic energy. Acta Oceanologica Sinica, 43(12): 1–12, doi: 10.1007/s13131-024-2365-0

1 Introduction

When studying the multiscale dynamics of the ocean, it is necessary to decompose the total flow into a steady or slowly varying mean-flow component (also called the background or basic flow) and a fluctuating, quickly varying perturbation (or eddy-flow) component, on the basis of a pre-defined separation scale. The budget of meanflow kinetic energy (MKE) and eddy kinetic energy (EKE) comprising their generation, dissipation, advection, and conversion is the centerpiece of ocean energetics (Penduff et al., 2004; von Storch et al., 2012; Chen et al., 2014, 2016; Kang and Curchitser, 2015). Different scale-separation methods (as known as flow-decomposition methods) result in different energy terms. Particularly, for some scale-separation methods, there exists a residual kinetic energy (RKE) term besides the MKE and EKE, complicating the analysis on cross-scale energy transfer. Recently, Zhou and Cheng (2021) (hereafter ZC21) examined theoretically the origin and properties of the RKE, and quantitatively assessed spatial distribution of the RKE in the global oceans using several separation methods on a range of spatial and time scales. It was shown that the RKE from commonly used methods could be large and significant.

There are different ways to deal with the RKE. One option is to keep the RKE and handle it explicitly together with MKE and EKE in the time-dependent energy budget formulated by Chen et al. (2014, 2016). Alternatively, to exactly eliminate RKE at any moment, strictly orthogonal scale separation methods such as the localized Multiscale Window Transform (Liang, 2012, 2016) must be employed. A compromise is to give up the instantaneity and turn to the mean energies using the conventional Reynolds mean (REM), taking advantage of the REM's ability to ensure orthogonality in the sense of time-mean, but meanwhile assuming invariant background flow. Filtering methods such as the universally employed running mean (RUM) could be used to allow varying background flow but is prone to the RKE which is usually assumed weak.

Recently, ZC21 proposed conceptually another method—the piecewise Reynolds mean (PREM). This method extends the conventional REM with a sliding window of a predefined length (or separation scale), similar as the RUM but calculates the energy terms in different ways. It can be regarded as a combination of REM and RUM, and therefore retains the features of both zero RKE and varying background flow. However, ZC21 did not elaborate on the principles, properties and formulae of the PREM method, which are now comprehensively introduced in this pa-

Foundation item: The National Natural Science Foundation of China under contract No. 42276002; the Fund of State Key Laboratory of Tropical Oceanography, South China Sea Institute of Oceanography, Chinese Academy of Sciences under contract No. LTO2201; the Fund of Key Laboratory of Marine Hazards Forecasting, Ministry of Natural Resources, China under contract No. LOMF2201.
*Corresponding author, E-mail: guidi.zhou@hhu.edu.cn

per, together with detailed intercomparison with the REM and RUM methods. Quantitative assessment of the energy terms and conversion rate from the PREM and RUM methods in the global oceans are also presented in terms of time mean and interannual variability, with an emphasis on mesoscale eddies.

Further, recently there appears another type of physics-oriented method, the eddy detection and extraction (EDEX), specially devised for energetics of mesoscale eddies. Two recently-proposed EDEX methods, i.e., those of Zhou et al. (2021b) and Bonaduce et al. (2021), are also introduced and compared with PREM. In total, this paper draws a rather thorough picture of the PREM and other methods in the context of multiscale energetics, with a focus on mesoscale eddies.

The remainder of this paper is organized as follows. Section 2 introduces the dataset. Section 3 lays the groundwork of defining the energy terms and conversion rate. Section 4 progressively introduces the REM, PREM, RUM, and EDEX methods in terms of their concept, properties, and mathematical forms. Section 5 quantitatively evaluates and compares the energy terms and conversion rate estimated by the PREM, RUM, and EDEX, showing global distributions of their time-mean, interannual variability, and method discrepancies. Section 6 provides summary and discussion.

2 Data

We use the geostrophic current velocity data from the AVISO project (Ducet et al., 2000) to estimate the kinetic energy terms and conversion rate based on three different scale-separation methods. The data cover the 28 years of 1993–2020, with a (1/4)° spatial resolution and a daily temporal resolution. This dataset has been widely used in studies on ocean mesoscale energetics. The climatological annual cycle is removed prior to any calculation.

3 Definition of energy terms and conversion rate

The total kinetic energy (TKE) of the 2-D flow field $\boldsymbol{u} = (u, v)$ is defined as follows:

$$\mathrm{TKE} = \frac{\rho_0}{2}\boldsymbol{u}^2 = \frac{\rho_0}{2}\left(u^2 + v^2\right), \tag{1}$$

where ρ_0=1 025 kg/m^3 is the reference density of seawater, u and v are the zonal and meridional components of the velocity vector, which can vary in space and time. In this work we follow common practice and regard time series at different spatial locations as individual observations, and thus focus only on the time domain.

Partition the total flow $\boldsymbol{u}$ using a certain scale-separation method (introduced later) into the mean-flow (or background) part and the perturbation (or eddy-flow) part as $\boldsymbol{u} = \overline{\boldsymbol{u}} + \boldsymbol{u}'$, the MKE and the EKE are defined accordingly as

$$\mathrm{MKE} = \frac{\rho_0}{2}\overline{\boldsymbol{u}}^2 = \frac{\rho_0}{2}\left(\overline{u}^2 + \overline{v}^2\right), \tag{2}$$

$$\mathrm{EKE} = \frac{\rho_0}{2}\boldsymbol{u}'^2 = \frac{\rho_0}{2}\left(u'^2 + v'^2\right). \tag{3}$$

Substituting the decomposition into the TKE, however, it is easy to find that there exists a third energy term, the RKE:

$$\mathrm{TKE} = \mathrm{MKE} + \mathrm{EKE} + \mathrm{RKE}, \tag{4}$$

where

$$\mathrm{RKE} = \rho_0\overline{\boldsymbol{u}}\boldsymbol{u}' = \rho_0\left(\overline{u}u' + \overline{v}v'\right). \tag{5}$$

Unlike the MKE and EKE, the RKE takes both positive and negative values.

The barotropic conversion rate (BTR) between the MKE and EKE is

$$\begin{aligned}\mathrm{BTR} &= -\rho_0\left(\overline{\boldsymbol{u}'\boldsymbol{u}'}\cdot\nabla\overline{u} + \overline{\boldsymbol{v}'\boldsymbol{u}'}\cdot\nabla\overline{v}\right)\\ &= -\rho_0\left(\overline{u'^2}\frac{\partial\overline{u}}{\partial x} + \overline{u'v'}\frac{\partial\overline{u}}{\partial y} + \overline{u'v'}\frac{\partial\overline{v}}{\partial x} + \overline{v'^2}\frac{\partial\overline{v}}{\partial y}\right),\end{aligned} \tag{6}$$

where the $\overline{\boldsymbol{u}'\boldsymbol{u}'}$ and $\overline{\boldsymbol{v}'\boldsymbol{u}'}$ vectors involve the terms $\overline{u'^2}$, $\overline{v'^2}$, and $\overline{u'v'}$, requiring application of the decomposition method, particularly the overbar operator, on the velocity variance terms u'^2, v'^2, and $u'v'$ in the same way as for u and v. The sign convention is such that positive BTR indicates forward energy cascade (MKE to EKE) and negative BTR indicates inverse cascade (EKE to MKE).

The above definitions of the energy terms and conversion rate are general and invariant, regardless of the chosen scale-separation method. However, as shown by ZC21, certain methods give orthogonal $\overline{\boldsymbol{u}}$ and $\boldsymbol{u}'$, causing RKE to vanish. Other methods give non-zero RKE, but could make it small in some circumstances.

4 Flow decomposition methods

4.1 *Reynolds mean*

Since the RKE causes complication in understanding the cross-scale energy transfer, it is usually favorable to design and adopt scale-separation methods that guarantee RKE = 0. Such methods would have $\overline{\boldsymbol{u}}\boldsymbol{u}' = 0$, meaning the mean-flow and the eddy flow are decomposed in an orthogonal way. Strict orthogonality on the time-dependent flow field can only be realized using sophisticated methods like the multiscale window transform (Liang, 2012, 2016; Yang and Liang, 2019), yet orthogonality in the sense of time-mean can be achieved using the much simpler conventional REM method.

The REM defines the mean-flow as the overall time-average of the observed discrete time series of velocity, i.e.,

$$\overline{\boldsymbol{u}} \doteq [\boldsymbol{u}] = \frac{1}{N}\sum_{i=1}^{N}\boldsymbol{u}_i, \tag{7}$$

where N is the number of observations. Note that here the overbar denotes the mean-flow, one of the two components of the total flow extracted by whichever method; and the square brackets are the Reynolds operator, essentially a statistical operator for the first moment, applied on observations of the total flow to extract the mean flow. The REM is often categorized as the statistical approach (Pope, 2000). The mean-flow defined by the Reynolds operator is constant in time, thus deviation from this constant is entirely assigned to the eddy-flow, i.e., $\boldsymbol{u}' \doteq \boldsymbol{u} - [\boldsymbol{u}]$.

It is easy to establish that the Reynolds operator has some good properties (Reynolds, 1895):

$$[[f]] = [f], \tag{8}$$

$$[f[g]] = [f][g], \tag{9}$$

$$[f \pm g] = [f] \pm [g], \tag{10}$$

with f and g denoting two arbitrary functions on the time domain. The key to these properties is the fact that the overall mean of any function is constant, and that the mean of constants equals themselves.

In this case, $\mathrm{RKE} = \rho_0 \overline{\boldsymbol{u}}\boldsymbol{u}' = \rho_0 [\boldsymbol{u}] (\boldsymbol{u} - [\boldsymbol{u}])$ is non-zero because generally $\boldsymbol{u} \neq [\boldsymbol{u}]$ (otherwise the flow field is constant), and thus must be considered in the instantaneous energy balance equations, which was strictly derived by Chen et al. (2016). However, if we apply the Reynolds operator once again on the instantaneous RKE, it vanishes nicely:

$$\begin{aligned}[\mathrm{RKE}] &= \rho_0 [[\boldsymbol{u}] (\boldsymbol{u} - [\boldsymbol{u}])] = \rho_0 \left[\boldsymbol{u} [\boldsymbol{u}] - [\boldsymbol{u}]^2\right] \\ &= \rho_0 \left([\boldsymbol{u} [\boldsymbol{u}]] - \left[[\boldsymbol{u}]^2\right]\right) = \rho_0 \left([\boldsymbol{u}]^2 - [\boldsymbol{u}]^2\right) = 0.\end{aligned} \tag{11}$$

It is therefore handy to study the energy cycle in the sense of time-mean, since it can be evaluated precisely in terms of just the [MKE] and [EKE] (e.g., von Storch et al., 2012). This time-mean energy cycle is universally known as the Lorenz cycle. The formulae of the [TKE], [MKE], [EKE], and [BTR] of the Lorenz cycle can be easily derived and are listed in the first column of Table 1.

4.2 *Piecewise Reynolds mean*

One of the limitations of the REM method is the attribution of all fluctuation to the perturbation or eddy term, prohibiting the background mean-flow from evolving. This is unfavorable in many applications, e.g., on dynamic interactions between intraseasonal mesoscale eddies with a background jet that varies significantly on interannual timescales. The eddy-jet interaction in the Kuroshio Extension region is a good example. To overcome this shortcoming while retaining the zero [RKE], ZC21 proposed the PREM method, which, as the nomenclature indicates, virtually performs the Reynolds mean on a moving window of a predefined length. The detailed procedure is explained in the following.

Consider a certain window of length $2L + 1$ (L is called the half-length) centered at the i-th sample of the observed record of length N. Without losing generality, assume N to be odd. Regard the window as a sub-record, and define the "mean-flow" in this window as the piecewise "Reynolds mean", i.e., the average of data points included in the window:

$$\langle \boldsymbol{u} \rangle_i = \frac{1}{2L+1} \sum_{j=-L}^{L} \boldsymbol{u}_{i+j}. \tag{12}$$

The subscript i denotes the i-th window, and j indicates the offset from the window center. The mean-flow is apparently constant within the window but varies across windows along the time coordinate. The angle bracket operator is therefore essentially the running meaning operator. In the case of $2L + 1 = N$, i.e., only one window in the entire record, PREM reduces to REM.

The MKE of window i can be calculated accordingly the formula as follows:

$$\mathrm{MKE}_i = \frac{1}{2} \rho_0 \langle \boldsymbol{u} \rangle_i^2. \tag{13}$$

The eddy velocity for each sample point within window i is derived as the deviation from the window-specific mean velocity:

$$\boldsymbol{u}'_{i+j} = \boldsymbol{u}_{i+j} - \langle \boldsymbol{u} \rangle_i, \quad j = -L, -L+1, \ldots, L. \tag{14}$$

Then the EKE_{i+j}, RKE_{i+j}, and BTR_{i+j} for each point can be similarly written out following Eqs (2), (3), (5), and (6).

Then, we give up the flexibility of instantaneous energy, and turn to the mean energy terms $\langle \mathrm{TKE} \rangle_i$, $\langle \mathrm{EKE} \rangle_i$, $\langle \mathrm{RKE} \rangle_i$, and $\langle \mathrm{BTR} \rangle_i$ for window i, each term getting just one value (MKE_i is already a constant in the window). This is equivalent to performing the REM on this specific window, therefore in this case the angle bracket operator $\langle \cdot \rangle$ has the same properties of the square brackets $[\cdot]$. Particularly, since eddy velocities $\boldsymbol{u}'_{i+j}$ in each window are referenced to a fixed mean velocity $\langle \boldsymbol{u} \rangle_i$, it is easy to deduce that $\langle \mathrm{RKE} \rangle_i = 0$, even though $\mathrm{RKE}_{i+j} \neq 0$. Move the window across the entire record (i.e., let i vary) and we get a series of energy terms for each window. The formulae of the energy terms and conversion rate are derived and shown in the second column of Table 1 with the subscript i omitted for conciseness. In practice, the calculation of EKE is simply a linear combination of $\langle u^2 \rangle$, $\langle v^2 \rangle$, $\langle u \rangle^2$, and $\langle v \rangle^2$, requiring only running-average of squared velocity and square of running-averaged velocity. BTR requires an additional term of $\langle uv \rangle$. The calculations can be efficiently implemented utilizing vectorization facilities of modern computers.

Unlike REM and RUM (see next subsection), in PREM the eddy velocity $\boldsymbol{u}'$ on each time-sample is calculated multiple

Table 1. Formulae of the mean energy terms and conversion rate using the REM, PREM, and RUM methods

Energy term	REM	PREM	RUM
$\frac{2}{\rho_0}\mathrm{TKE}$	$[u^2] + [v^2]$	$\langle u^2 \rangle + \langle v^2 \rangle$	$\langle u^2 \rangle + \langle v^2 \rangle$
$\frac{2}{\rho_0}\mathrm{MKE}$	$[u]^2 + [v]^2$	$\langle u \rangle^2 + \langle v \rangle^2$	$\langle \langle u \rangle^2 \rangle + \langle \langle v \rangle^2 \rangle$
$\frac{2}{\rho_0}\mathrm{EKE}$	$[u^2] - [u]^2 + [v^2] - [v]^2$	$\langle u^2 \rangle - \langle u \rangle^2 + \langle v^2 \rangle - \langle v \rangle^2$	$\langle u^2 \rangle + \langle \langle u \rangle^2 \rangle - 2\langle u\langle u \rangle \rangle + \langle v^2 \rangle + \langle \langle v \rangle^2 \rangle - 2\langle v\langle v \rangle \rangle$
$\frac{1}{\rho_0}\mathrm{RKE}$	0	0	$\langle u\langle u \rangle \rangle - \langle \langle u \rangle^2 \rangle + \langle v\langle v \rangle \rangle - \langle \langle v \rangle^2 \rangle$
$\frac{1}{\rho_0}\mathrm{BTR}$	$\left([u^2] - [u]^2\right) \frac{\partial [u]}{\partial x} +$ $([uv] - [u][v]) \left(\frac{\partial [u]}{\partial y} + \frac{\partial [v]}{\partial x}\right) +$ $\left([v^2] - [v]^2\right) \frac{\partial [v]}{\partial y}$	$\left(\langle u^2 \rangle - \langle u \rangle^2\right) \frac{\partial \langle u \rangle}{\partial x} +$ $\left(\langle uv \rangle - \langle u \rangle \langle v \rangle\right) \left(\frac{\partial \langle u \rangle}{\partial y} + \frac{\partial \langle v \rangle}{\partial x}\right) +$ $\left(\langle v^2 \rangle - \langle v \rangle^2\right) \frac{\partial \langle v \rangle}{\partial y}$	$\left\langle \langle (u - \langle u \rangle)^2 \rangle \frac{\partial \langle u \rangle}{\partial x} \right\rangle +$ $\left\langle \langle (u - \langle u \rangle)(v - \langle v \rangle) \rangle \frac{\partial \langle u \rangle}{\partial y} \right\rangle +$ $\left\langle \langle (u - \langle u \rangle)(v - \langle v \rangle) \rangle \frac{\partial \langle v \rangle}{\partial x} \right\rangle +$ $\left\langle \langle (v - \langle v \rangle)^2 \rangle \frac{\partial \langle v \rangle}{\partial y} \right\rangle$

Note: The terms in the first column are averaged over the entire record in REM and are therefore time-independent (i.e., the $[\cdot]$ operator is applied); and running-averaged over a moving window of a pre-defined length in PREM and RUM (i.e., the $\langle \cdot \rangle$ operator is applied).

times. For example, let L be, say, 3, then the 12th sample point is included in seven windows ($i = 9, 10, \ldots, 15$), each including seven points (Fig. 1a). The eddy velocity at this point, $\boldsymbol{u}'_{12}$, is calculated seven times as $\boldsymbol{u}'_{9+3} = \boldsymbol{u}_{9+3} - \langle \boldsymbol{u} \rangle_9$, $\boldsymbol{u}'_{10+2} = \boldsymbol{u}_{10+2} - \langle \boldsymbol{u} \rangle_{10}, \ldots, \boldsymbol{u}'_{15-3} = \boldsymbol{u}_{15-3} - \langle \boldsymbol{u} \rangle_{15}$, each time using the same total velocity $\boldsymbol{u}_{12}$ but referenced to different mean-flow velocity $\langle \boldsymbol{u} \rangle_9, \langle \boldsymbol{u} \rangle_{10}, \ldots, \langle \boldsymbol{u} \rangle_{15}$. Those seven values of $\boldsymbol{u}'_{12}$ are finally used separately to compute the respective $\langle \mathrm{EKE} \rangle_i$ and $\langle \mathrm{RKE} \rangle_i$ for window 9 through window 15, together with other members of each window. However, this procedure is only conceptual, because in practice the energy terms can be directly calculated following our simplified formulae in Table 1.

The energy terms obtained by this method are mean energies over a certain period of $2L + 1$, and are thus different to either the REM, the instantaneous energies, and the results of other decomposition methods. First, they are time-varying instead of time-constant, an improvement over the REM. Second, they represent the mean state of energy spanning a certain period centering at a specific time, instead of the exact energy at that particular moment. This may seem like a drawback compared to strictly orthogonal decomposition methods, but the present method is much easier to implement. Third, due to the retaining of mean orthogonality, this method does not suffer from the RKE that complicates the calculation and interpretation of the energy cycle, which is advantageous over other methods that compromise both orthogonality and instantaneity, as is about to be discussed.

4.3 *Running mean*

Traditional scale-separation methods other than the REM are often categorized as the filtering approach. They rely on certain kinds of filters to extract Fourier harmonics on frequencies within the "passband" and suppress those in the "stopband" in the spectral domain. Using a lowpass filter, e.g., the resultant low-frequency component is often treated as the time-dependent mean-flow or background flow, and the deviation from it as the eddy-flow or fluctuation.

Empowered with the convolution theorem, filters are usually implemented by convolution of the original time series with a kernel function for computational efficiency and flexibility. Convolution is practically equivalent to applying a running mean weighted by the kernel function on the observed time series, and is also analogous to multiplying the spectrum of the kernel function (called the response function) to the spectrum of the data. A kernel function, or a filter, is considered perfect if its response function has unit value in the passband and zero in the stopband, thus returning clear-cut mean-flow and eddy components. Since the sole perfect kernel function, the sinc function, only exists for infinite continuous time series, in practical finite discrete scenarios the separated flow components are always interdependent to some extent, giving rise to non-zero RKE. Refer to ZC21 for more details on filter design.

The simplest kernel function is the boxcar (or top hat) function, which is equivalent to performing an unweighted running mean with certain window length. Albeit its response function is far from ideal, it is still universally used thanks to its conceptual and computational easiness. Here we choose the boxcar kernel filter, as known as RUM method as a representative of the filtering approach to compare with the PREM method for the sake of easy mathematical derivation of the energy terms.

The RUM method defines the mean-flow in the same way as the PREM, i.e., as running-averaged velocity Eq. (12). The difference between these two methods is manifested in the definition of the eddy velocity. Unlike the PREM, the RUM treats the eddy flow as the direct difference between the total and mean-flow at each individual time step:

$$\boldsymbol{u}_i{}' = \boldsymbol{u}_i - \langle \boldsymbol{u} \rangle_i, \tag{15}$$

which is very easy and thus commonly employed in studies of cross-scale energy cycle (Jia et al., 2011; Jouanno et al., 2012; Kang and Curchitser, 2017; Wang and Yu, 2018). For instance, $\boldsymbol{u}'_{12} = \boldsymbol{u}_{12} - \langle \boldsymbol{u} \rangle_{12}$, and $\boldsymbol{u}'_{13} = \boldsymbol{u}_{13} - \langle \boldsymbol{u} \rangle_{13}$, etc., each calculated only once, referencing to different mean velocities. See Fig. 1b for a schematic explanation. In fact, this procedure is equivalent to having the window length in Eq. (14) shrunk to 1 when calculating the eddy velocity, effectively cancelling the separate calculation of eddy velocity for each sample in the window. However, since the running mean process for calculating the mean-flow Eq. (12) still has a non-trivial window length, for conceptual clarity it is beneficial to distinguish between the two windows and denote the half-lengths in Eqs (12) and (14) using different symbols. Here we keep L for Eq. (12) and use M for Eq. (14). Thus, in PREM $M = L \neq 0$ but in RUM $M = 0$.

The energy terms are then calculated accordingly from the velocities. Because $M = 0$, they are not actually averaged across a certain window, but take instantaneous values. However, the readers are reminded that in PREM the target is the mean energy terms over a certain period; hence the instantaneous energy in RUM will certainly consist of higher level of variability than in PREM. To ensure fair comparisons with PREM, another running mean must be performed on the energy terms. This additional running mean is labeled with half-length T for clarity, and T should equal M or L of PREM for comparability. Within each T-window centered at i,

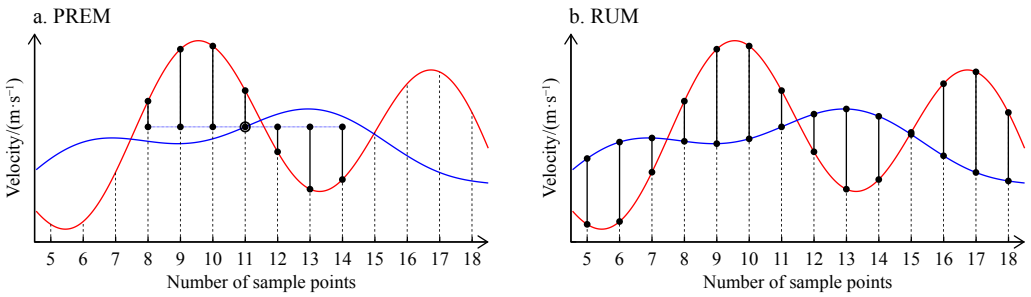

Fig. 1. Schematic diagram of the PREM (a) and RUM (b) methods. Red curves are the original time series of velocity, and blue curves are the running-averaged velocity. Black bars with dots denote the perturbation velocity (difference between original and running-average) used for calculating the EKE within each window (in RUM the window size is unity).

$$\frac{\mathrm{RKE}_{i+j}}{\rho_0} = \boldsymbol{u}_{i+j}\langle\boldsymbol{u}\rangle_{i+j}^{L} - \langle\boldsymbol{u}\rangle_{i+j}^{L^2}, \quad j = -T,\ -T+1,\ \ldots,\ T, \tag{16}$$

where $\langle\boldsymbol{u}\rangle_{i+j}^{L}$ is the L-window-mean velocity resulting from Eq. (12). Here, the $\langle\boldsymbol{u}\rangle_{i+j}^{L}$ are not constant for different j in the T-window, thus $\left\langle \boldsymbol{u}\langle\boldsymbol{u}\rangle^{L}\right\rangle^{T} \neq \langle\boldsymbol{u}\rangle^{L^2}$ and $\left\langle \langle\boldsymbol{u}\rangle^{L^2}\right\rangle^{T} \neq \langle\boldsymbol{u}\rangle^{L^2}$, and consequently $\langle\mathrm{RKE}\rangle_i^{T} \neq 0$. In contrast, in PREM the RKE_{i+j} in the i-th M-window is proportional to $\boldsymbol{u}_{i+j}\langle\boldsymbol{u}\rangle_i^{L} - \langle\boldsymbol{u}\rangle_i^{L^2}$, where $\langle\boldsymbol{u}\rangle_i^{L}$ is independent of j by design, which is why $\langle\mathrm{RKE}\rangle_i^{M} = 0$. Such difference is apparently rooted in the relative order of the windowing and energy calculation operations. In PREM energy calculation is performed after taking the M-window which ensures constant window-specific mean velocity; while in RUM the M-window is skipped ($M = 0$) and energy is calculated before taking the T-window, which virtually includes multiple single-sample M-windows each having different mean velocities.

The energy terms resulting from the RUM are listed in the last column of Table 1.

4.4 *Eddy detection and extraction*

The above methods are all based on statistics or filters, relying on a window length chosen a priori to separate the larger-scale mean-flow and the smaller-scale perturbations. Such window length or separation scale is chosen according to the typical scales of the phenomenon under study. For the study of midlatitude mesoscale eddies, which are rotating circular vortices, the separation scale is usually set to around a year, in acknowledgement that mesoscale eddies typically live for weeks or months. Such a procedure, albeit certainly useful, is subject to some difficulties. First, the fixed separation scale is not adaptive to all the intended physical process. Some mesoscale eddies, e.g., those in the eastern subpolar North Pacific, are known as long-living and quasi-permanent (e.g., Di Lorenzo et al., 2005; Saito et al., 2014) and are thus not detectable using the one-year window. To avoid missing out longer-living eddies than the chosen timescale, the separation scale must be elongated. This, however, worsens the next problem. Second, there are often different types of physical processes on similar scales. For instance, besides mesoscale eddies, oceanic fronts and jet stream meanders are also mesoscale features which cannot be precluded from the filtered flow field (Liu et al., 2007; Qiu et al., 2014; Zhou et al., 2021a; Zhou and Cheng, 2022). As a result, the extracted eddy-flow actually consists of processes other than mesoscale eddies, and should therefore be strictly referred to as "mesoscale perturbations" or variability etc. Often, we either treat these phenomena as a whole assuming similar mechanisms and roles in the energy cycle, or implicitly consider only the mesoscale eddies presuming their dominance over other processes.

Pure and adaptive decomposition of mesoscale eddies from the total flow field could be accomplished by EDEX. Several kinds of techniques have now been available for eddy detection, based on either dynamical (sea level or velocity anomaly) or thermodynamical (sea surface temperature) perspectives, objective or parametric. One of the most widely used technique is to find the outermost closed sea level anomaly contour around local maxima (Faghmous et al., 2015). The outermost closed contours are marked as eddy boundaries. Next, the sea level anomaly induced by the eddy must be extracted from the background. A few methods have recently been developed for this purpose. In this work we use the two methods proposed by Zhou et al. (2021b) and Bonaduce et al. (2021).

The concept of the Zhou et al. (2021b) method is to first determine the eddy amplitude as the sea level difference between the maxima inside the eddy and the mean in the ambient. The ambient is defined as outside the eddy but within 3 times the eddy radius. The eddy-induced sea level anomalies on each grid point of the eddy body are then linearly interpolated from the eddy amplitude at the center toward zero at the boundary. The method Bonaduce et al. (2021) first fills the outermost grid points in the eddy with the average over a certain number of nearest grid points outside the eddy, and then progressively fills inner points in the same way until the whole eddy is filled. This procedure extrapolates the background into the eddy, and the eddy field is then extracted by subtracting the background from the original. In both methods, pure eddy-induced sea level and thereby geostrophic velocity anomalies are obtained, with no assumptions on eddy scale or lifespan whatsoever. EKE is then calculated from the eddy velocity.

The EDEX method has some drawbacks too. First, there is no mathematical form for the extracted eddy velocity. However, EKE and other energy terms can still be calculated based on Eq. (3) etc. Second, it leaves other mesoscale features besides eddies to the background flow, thus exaggerating the MKE. Third, the eddy detection and extraction algorithms are prone to their own errors. Particularly, the definition of the eddy boundary as the outermost sea level contour is not necessarily optimal, and the definition of the "background" around the eddies is also a matter of opinion. Last, the filtering methods are easily adjustable to other types of phenomena by simply changing the separation scale (which, as discussed above, have problems), while the EDEX only works for mesoscale eddies. Particularly, the sea level-based algorithm excludes ageostrophic flows that might be present with submesoscale processes near the eddy perimeter.

Nevertheless, it is interesting and advantageous to intercompare the two completely different categories of flow decomposition methods, especially given our primary interest in mesoscale eddy energetics. As in the case of the PREM-RUM intercomparison, a running mean should be performed on the EKE resulting from EDEX, given that PREM aims at mean energies but EDEX evaluates instantaneous EKE on each time stamp.

5 Intercomparison of PREM, RUM, and EDEX

5.1 *PREM vs. RUM: time-mean energy terms*

In this section we present intercomparison of the energy terms deduced using the PREM and RUM methods based on satellite-derived surface geostrophic current velocity. Here we focus on intra-annual variability defined as fluctuations on timescales shorter than 1 year. Therefore, in PREM $M = L = 1$ year, and in RUM $L = T = 1$ year and $M = 0$. The energy terms MKE, EKE, and BTR are compared in terms of time-mean and interannual variability.

The 28-year mean MKE estimated by the PREM is shown in Fig. 2a. The three strongest currents, i.e., the Kuroshio Extension, the Gulf Stream Extension, and the Agulhas Return Current are easily visible, with maximum MKE of over 60 J/m^3. Other western boundary regions, i.e., the North Pacific Current, and the Antarctic Circumpolar Current (ACC), also exhibit strong MKE. In the time-mean, the maximum difference of MKE between the PREM and RUM methods is on the order of 1 J/m^3 (Fig. 2b) or about 5% relative to RUM (Fig. S1a). In the extratropical strong current regions, there are interlacing positive and negative differences, while in the tropics the differences are mostly positive.

The time-mean intra-annual EKE, as shown in Fig. 2c, high-

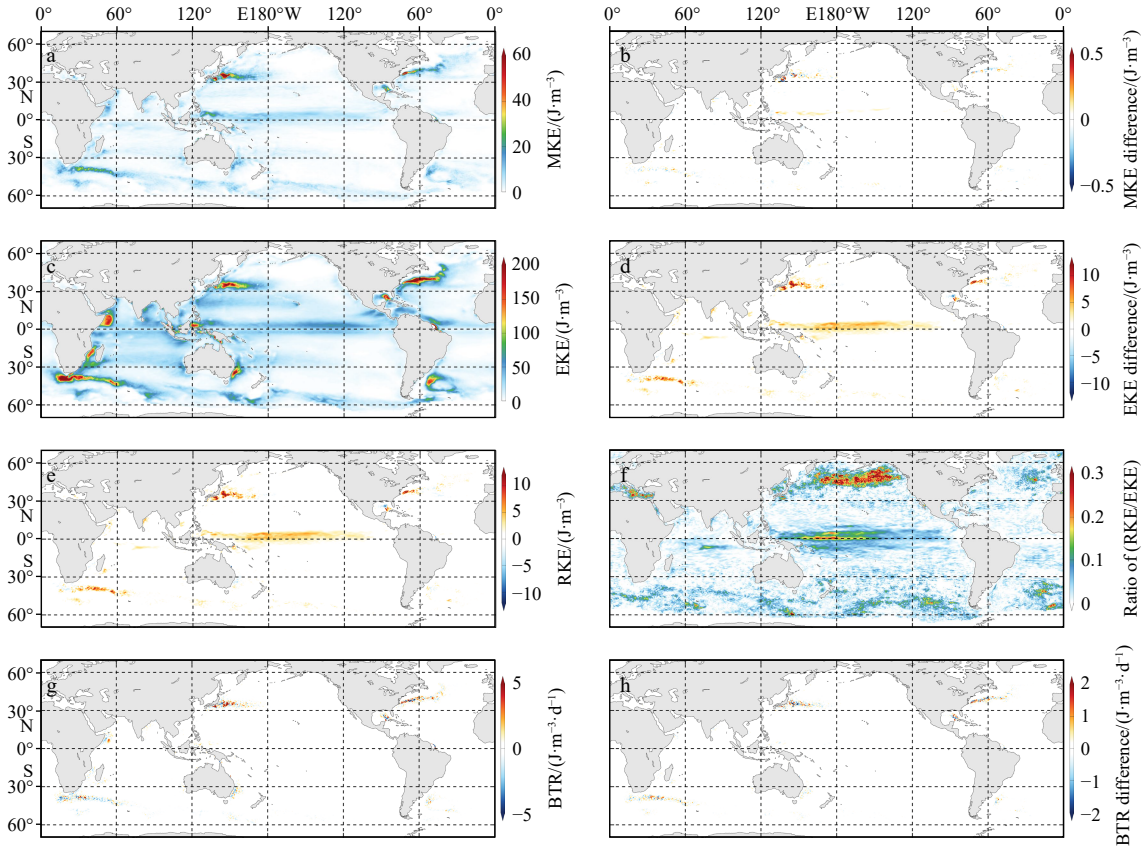

Fig. 2. Comparison of 28-year averaged energy terms and conversion rate estimated by the PREM and RUM methods. a. MKE of the PREM method; b. MKE difference of PREM-RUM; c. EKE of the PREM method; d. EKE difference of PREM-RUM; e. RKE of the RUM method; f. ratio of RKE/EKE of the RUM method; g. BTR of the PREM method; h. BTR difference of PREM-RUM.

lights the eddy-rich Kuroshio and the Gulf Stream Extensions, the Agulhas Return Current, the western boundary currents of the Southern Hemisphere, and a few marginal seas: the Gulf of Mexico, the Celebes Sea, the Amazon Estuary (North Brazil Current Retroflection), and the western Indian Ocean off Somalia (Somali Current). High energy is also found along the ACC, the Subtropical Countercurrents in both hemispheres, and both flanks of the equator. Maximum EKE exceeds 200 J/m^3, making up the most energetic part of ocean motions. Along the eastern, northern, and northwestern boundary of North Pacific, there is also a band of relatively high EKE, which is associated with conversion from boundary Kelvin waves to Rossby waves (e.g., Clarke, 1983; Fu and Qiu, 2002), and the generation and propagation of Gulf of Alaska eddies, Aleutian eddies, and Kuril eddies (Rogachev et al., 2007; Saito et al., 2014; Rogachev and Shlyk, 2018, 2019). In the eastern North Atlantic, a line of relatively high EKE is detectable from the Strait of Gibraltar extending into the ocean, essentially a surface signature of the "meddies" which maximize in the subsurface, causing fluctuations on the intra-annual timescale (Zenk et al., 1992; Bower et al., 1995, 1997; Paillet et al., 2002; Serra and Ambar, 2002; Serra et al., 2005; Drillet et al., 2005). Compared with PREM, the RUM method systematically underestimates the mean EKE by up to 33 J/m^3 (Fig. 2d, maximizing in the Kuroshio Extension), except for in a few locations including the northern Gulf of Mexico where the PREM gives smaller EKE than RUM.

The mean RKE of the RUM method is shown in Fig. 2e, which mostly resembles Fig. 2d. This is expected because by definition, the RKE equals ($\mathrm{MKE_{PREM}}$–$\mathrm{MKE_{RUM}}$) plus ($\mathrm{EKE_{PREM}}$–$\mathrm{EKE_{RUM}}$), and the latter prevails. Physically this indicates that the non-orthogonal scale-separation, and therefore the additional residual energy, harms the EKE the most. It is further noteworthy from Fig. 2f and Fig. S1b that although the RKE has small absolute values in weak current regions, it does account for a non-negligible fraction of the intra-annual EKE in areas like the subpolar central and eastern North Pacific where the proportion reaches 48%, as well as in the eastern North Atlantic, the Mediterranean, the central and western Tropical Pacific, and spots in the ACC. When analyzing the cross-scale energy budget in these regions, the ignorance of the RKE could cause severe bias of the results, and therefore must be handled carefully. Western boundary current regions are generally less prone to the RKE, but the percentage of RKE/EKE can still reach 20%–30% in e.g., the Kuroshio south of Japan, upstream Kuroshio Extension, Oyashio Extension, and upstream Gulf Stream Extension.

It is useful to emphasize again that these results depend on the predetermined 1-year separation scale. Particularly, as pointed out by ZC21, the RKE/EKE ratio exhibits zonal distributions on the first order. The magnitude and latitude of the high RKE/EKE zone will be different for other separation scales (i.e., other values of L), a reflection of the latitudinal-dependence of the Rossby radius of deformation. Comparison of the PREM and RUM methods on other scales, e.g., subseasonal and interannual, is beneficial but not done in this paper for the sake of conciseness.

Figure 2g shows the time-mean barotropic conversion rate BTR from PREM, where positive (red) means forward cascade and negative (blue) means inverse cascade. It is directly inferable that in the time-mean, forward cascade is crucial for driving

the intra-annual eddy flow in the high-EKE regions of the Kuroshio and Gulf Stream extensions. However, the inverse cascade, i.e., energy feedback from the intra-annual perturbations to the mean-flow, is just as important (Qiu and Chen, 2010; Yang and Liang, 2016; Zhou et al., 2021a). The Somali Current, the Gulf of Mexico, the Eastern Australian Current, the Brazil Return Current, and the Brazil-Malvinas Confluence exhibit equally important forward and inverse cascades, indicating the role of cross-scale interaction between the mean-flow and eddies in maintaining their respective time-mean states. Inverse cascade predominates in some other regions, typically the Agulhas Return Current, while prevalence of forward cascade is found in the Celebes Sea and the northwestern Bay of Bengal (Chen et al., 2015; Cheng et al., 2018). Further, the maximum difference of BTR between PREM and RUM (Fig. 2h) is on the order of about half the mean BTR, taking both positive and negative values.

The above results demonstrate that the PREM and RUM methods do give significantly different time-mean energy terms, especially in terms of EKE and BTR in strong current regions.

5.2 *PREM vs. RUM: interannual variability*

Next, interannual variability of the energy terms is examined and compared between the PREM and RUM methods, measured by interannual standard deviation after removing the climatological annual cycle. As shown in Fig. 3a, the interannual variability of MKE estimated by PREM exhibits similar spatial distribution as the mean MKE, indicating stronger variation superimposed on stronger mean state. In many places, particularly the tropical Indian Ocean and the tropical eastern Pacific, the magnitude of the standard deviation exceeds two times the mean, while elsewhere it is almost always no less than the mean (Fig. S2a). Such strong interannual variability is severely underestimated in RUM by as much as 30 J/m^3 (Fig. 3b) or 120% (Fig. S2b).

The pattern of interannual standard deviation of intra-annual EKE largely follows that of the mean EKE (Fig. 3c). In strong current regions including the Kuroshio and Gulf Stream extensions, the Agulhas Return Current, and the equatorial central Pacific, the interannual variability of EKE is on the same order as the mean (Fig. S2c). Near the subpolar eastern boundary in the Gulf of Alaska and along the southern flank of the Aleutian Islands, the standard deviation is over 2 times the mean which is reflective of the strong and intermittent EKE variability associated with the near-stationary Haida, Sitka, Yakutat, and Aleutian eddies (Rogachev et al., 2007; Saito et al., 2014; Rogachev and Shlyk, 2018, 2019). In the Somali Current, the Celebes Sea, and the Eastern Australian Current, in contrast, the ratio is much lower, indicating relatively steady eddy activity across the years. The difference between PREM and RUM, as shown in Fig. 3d, reveals that RUM severely reduces interannual variability of EKE in most of the high-EKE regions. The maximum difference is 37 J/m^3 appearing in the Kuroshio Extension, which accounts for 108% of the local RUM result, while the global maximum percentage is 180% (Fig. S2d). The suppressed MKE and EKE variability in RUM is unsurprisingly taken up by RKE, which is evident from Figs 3e and f. Moreover, barotropic conversion rate BTR also exhibits remarkable interannual variability with standard

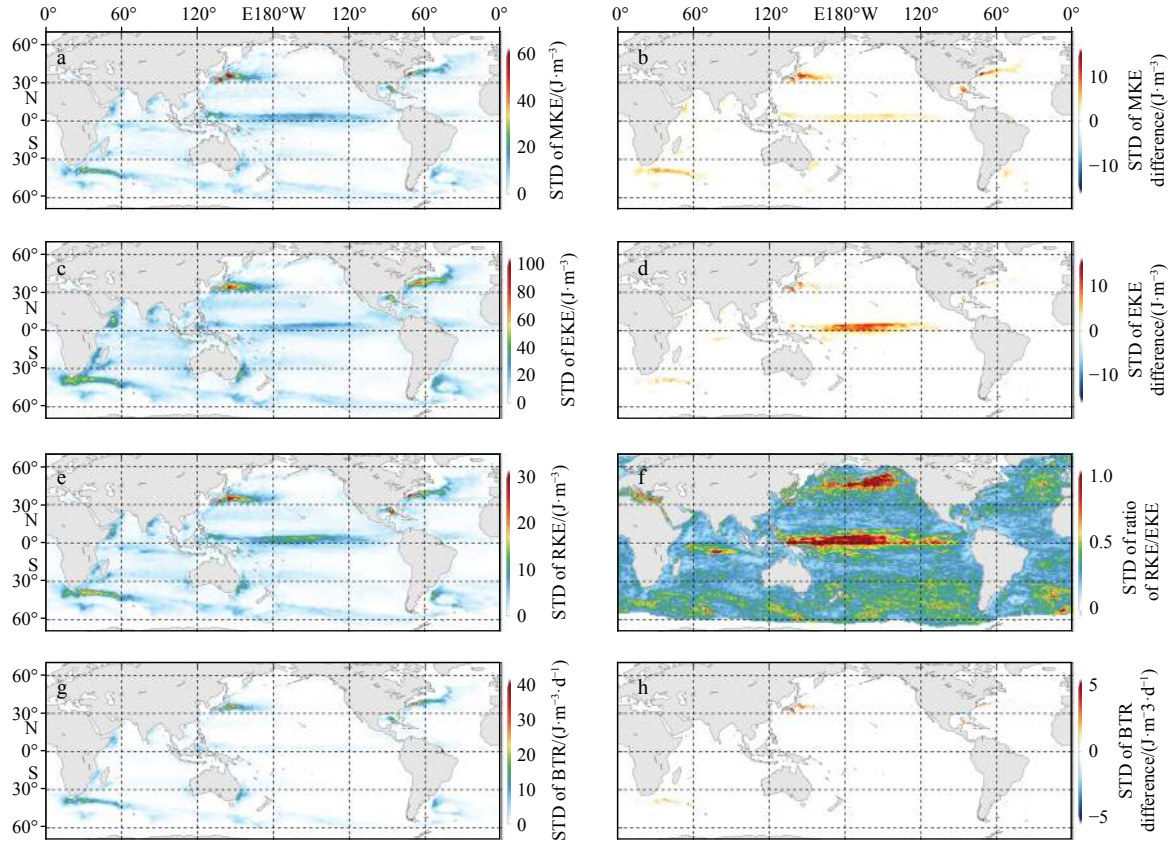

Fig. 3. Comparison of interannual standard deviation (STD) of energy terms and conversion rate estimated by the PREM and RUM methods. a. MKE of the PREM method; b. MKE difference of PREM-RUM; c. EKE of the PREM method; d. EKE difference of PREM-RUM; e. RKE of the RUM method; f. ratio of RKE/EKE of the RUM method; g. BTR of the PREM method; h. BTR difference of PREM-RUM.

deviation pattern resembling that of EKE (Fig. 3g). Difference between PREM and RUM again reveals underestimation of BTR variability by RUM in Kuroshio and Gulf Stream extensions, with slight overestimation downstream (Fig. 3h).

So far, we investigated the magnitude of interannual variability in terms of standard deviation. In the following, discrepancies between the two methods are evaluated in terms of root-square-mean difference (RMSD) and correlation, the former for magnitude conformity and the latter for phase agreement. The results for RMSD are shown in Fig. 4. It is not surprising to notice that the RMSD for the MKE, intra-annual EKE, and BTR terms exhibit similar spatial pattern as their mean and standard deviation (Figs 4a, c, and e), and it is useful to learn that the maximum RMSD can be as high as 46 J/m^3 (MKE), 60 J/m^3 (EKE), and 27 J/(m^{-3}·d) (BTR), respectively, much larger than the standard deviation difference. Maximum relative RMSD normalized by standard deviation (Figs 4b, d, and f) reach 180% (MKE), 208% (EKE), and 820% (BTR), highlighting different regions. Particularly, relative RMSD of intra-annual EKE in the Kuroshio and Gulf Stream Extensions is 154% and 80% of the respective standard deviation. These results emphasize the remarkable discrepancies between the two methods regarding the magnitude of the energy terms.

Figure 5 shows correlation coefficient between MKE, EKE, and BTR estimated by the PREM and RUM methods. High correlation indicates phase correspondence. Regarding MKE (Fig. 5a), the correlation is generally high in strong current regions, but can be lower than 0.7 in some areas. High correlation of EKE (Fig. 5b) is found in most of the global ocean, except for the subpolar basins and the tropics where correlation falls to 0.38. Along the narrow jets of the Kuroshio and Gulf Stream extensions, however, correlations smaller than 0.66 is noticeable. The spatial pattern of correlation of BTR (Fig. 5c) largely resembles that of EKE, but the phase mismatch is even worse in some regions. It is therefore conclusive that the discrepancies between the two methods in terms of both magnitude and phase are remarkable. Albeit the western boundary currents and other high-EKE regions are not the most affected, the absolute differences of the two methods are still large there. Hence, caution should be taken when studying interannual variability of the energy terms using RUM or similar filtering methods.

5.3 *PREM vs. EDEX*

The EDEX method is then employed based on detection of mesoscale rotating eddies (vortices) from altimeter-observed sea level anomalies following Faghmous et al. (2015), combined with the eddy field extraction method of Zhou et al. (2021b). The extracted eddy field is in terms of sea level anomalies and geostrophic velocities are calculated thereby. The tropical band between 5° north and south of the equator is omitted due to the near-zero Coriolis parameter. Since the eddy extraction method does not give the background flow, only EKE can be evaluated. We also tested an alternative eddy field extraction method developed by Bonaduce et al. (2021) which provides both the eddy and background flow fields. Results from the Zhou et al. (2021b) method are shown in Fig. 6, and those from the Bonaduce et al. (2021) method (denoted as EDEX-B) are included in Fig. S3.

It is easy to understand that the filtering approach (PREM and RUM) selects processes according to their timescale regardless of their physical nature, whereas EDEX detects and extracts mesoscale rotating vortices only, regardless of their timescale. The two types of methods thus assess energy of different physical processes, and are, in general, not directly comparable. However, it is known that mesoscale eddies do dominate surface intra-annual variability in mid-to-high latitude oceans, especially near the western boundary currents. Comparison between EDEX and PREM with $L = 1$ year is therefore meaningful and useful. Eddies tend to have shorter lifespan in lower latitudes and longer in higher latitudes (Cheng et al., 2014), hence accounting for a particular portion of intra-annual variability there, which is supposedly weaker than in the midlatitude.

Comparing Fig. 6a (EDEX) and Fig. 2c (PREM), it is evident

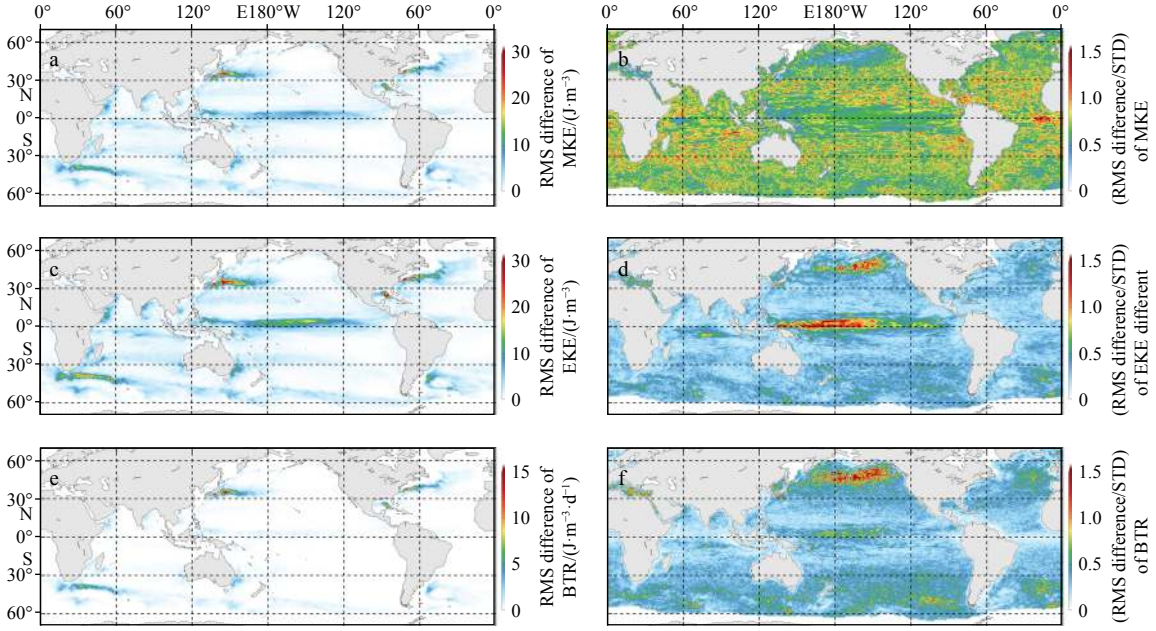

Fig. 4. Root-mean-square (RMS) difference between the energy terms and conversion rate estimated by the PREM and RUM methods. Left column, a, c and e. RMS difference; right column, b, d, and f. RMS difference divided by standard deviation of the energy term estimated by the RUM method. The energy terms are MKE (top row, a and b), EKE (middle row, c and d), and BTR (bottom row, e and f).

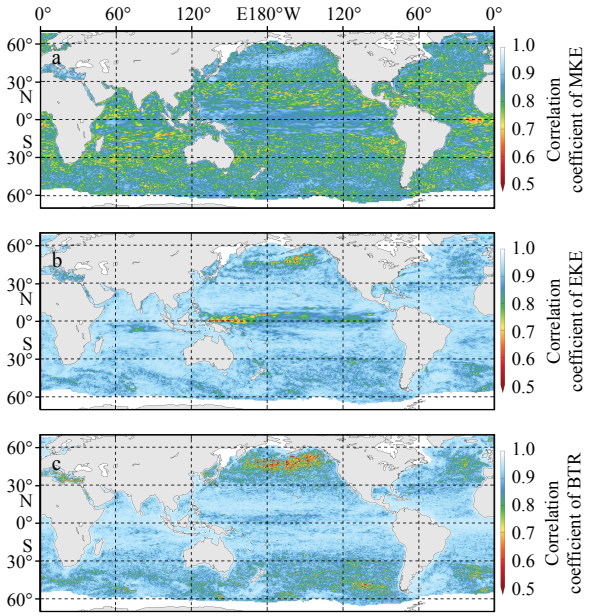

Fig. 5. Correlation between the energy terms and conversion rate estimated by the PREM and RUM methods. The energy terms are MKE (a), EKE (b), and BTR (c).

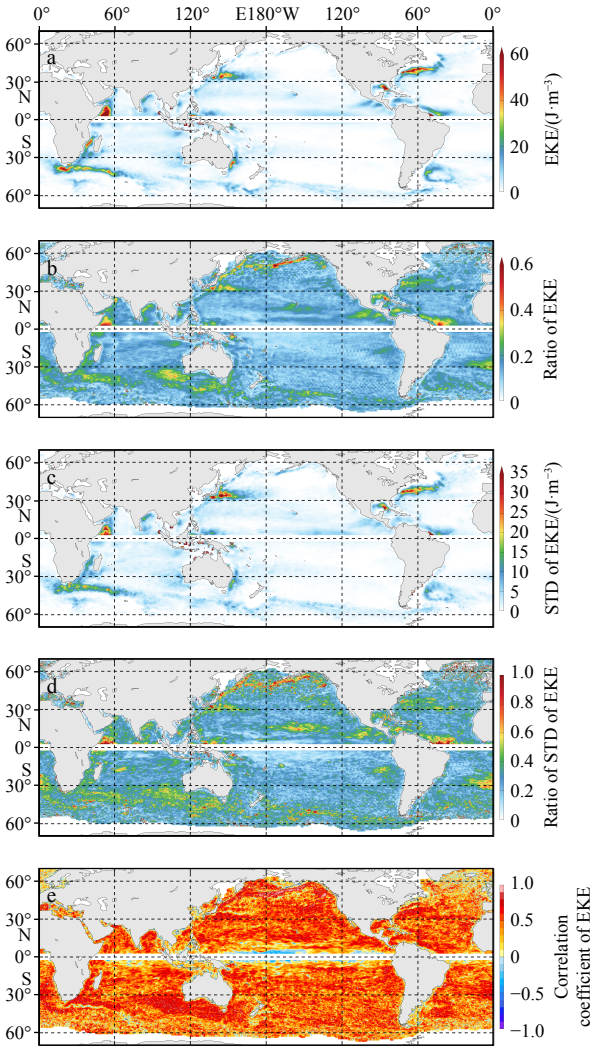

Fig. 6. 28-year averaged EKE (J/m^3) estimated by the EDEX method (a), fraction of 28-year averaged EKE of the EDEX method relative to the PREM method (b), interannual standard deviation of EKE of the EDEX method (c), fraction of interannual standard deviation of the EDEX method relative to the PREM method (d), and correlation of EKE of the EDEX and PREM methods (e).

that the time-mean EKE patterns from the two methods are indeed very similar. EDEX, however, gives weaker mean EKE, which is expected. As shown in Fig. 6b, in the Kuroshio Extension, Gulf Stream Extension, Somali Current, North Brazil Retroflection, and along the Aleutian and Kuril Islands, mean EKE estimated by EDEX accounts for 50%–80% of the PREM result, while in other eddy-active regions the fraction is on the order of 20%–40%. Considering the fact that in EDEX, eddy velocity (and thus EKE) at a certain grid point is exactly zero when it is not occupied by an eddy, it is comprehensible that the average EKE over a large number of zero values would of course be smaller, whereas in PREM zero EKE seldom occurs. PREM additionally includes non-circular perturbations that are not detected as mesoscale rotating eddies in EDEX. The relatively high percentage nevertheless confirms the dominance of mesoscale eddies. The smaller fraction in tropical and subtropical oceans is indicative that a fixed separation scale of 1 year used in PREM includes a bigger abundance of non-eddy processes.

The level of interannual EKE variability estimated from the two methods also exhibits high pattern resemblance (Figs 6c and 3c). The distribution of EDEX/PREM fraction (Fig. 6d) follows the same pattern as for mean EKE (Fig. 6b) but is generally higher. In eddy-rich regions the fraction approaches 1, suggesting that a large portion of the interannual variability of EKE is indeed controlled by mesoscale eddies. In terms of the phase of EKE interannual variability, as inferable from Fig. 6e, the EDEX and PREM methods generally agree, except for in some tropical and subpolar areas where weak and/or negative correlation is present. The low-latitude negative correlation is attributable to the non-eddy intra-annual processes in PREM because of the short lifespan of mesoscale eddies there, reflecting the cross-scale interaction. Perhaps somewhat surprisingly, along the thin jets of Kuroshio Extension, Gulf Stream Extension, and Agulhas Return Current, the correlation is negative (better seen from the high-resolution digital version of the figure). This might be a result of the mesoscale eddies being generated on both sides of, instead of exactly on, the jets. The EDEX thus gives low mesoscale eddy energy there when along-jet fronts and large meanders that are on the same scale of mesoscale eddies are strong, giving rise to high PREM EKE. The negative correlation between these eddy and non-eddy mesoscale features found here is an interesting topic for future research.

The EDEX-B method, moreover, produces similar mean EKE and standard deviation patterns, except that the very strong center in the Somali Current region is absent (Fig. S3). There, the part of energy missing from the EKE is relocated to the MKE, an effect of the different definition of "background" than in EDEX. Since the Somali Current eddy-active region is real (Beal and Donohue, 2013; Akuetevi et al., 2016; Seo, 2017; Trott et al., 2017; Wang et al., 2019), the EDEX method is seemingly superior to the EDEX-B. Correlations of both MKE and EKE with the PREM results are predominately high, while negative EKE correlation is still present in the low-latitudes but not along the strong jet currents (there the correlation is now weak but positive). Figure S4a presents the ratio of time-mean EKE of the EDEX and EDEX-B

methods in logarithmic scale. It is evident that EDEX-B severely underestimates the time-mean EKE in tropical and subtropical oceans and in the western midlatitudes, and overestimates EKE in subpolar oceans in both hemispheres and in the eastern ocean basins. Basically, EDEX-B lessens the high time-mean EKE and increases the low. Interannual variability of EKE (Fig. S4b), however, is intensively attenuated over much of the global oceans with maximum underestimation of over 1/10. The EDEX-B, therefore, gives spatially smoother and temporally steadier EKE than the EDEX.

6 Summary and discussion

Because of the possible existence of the RKE alongside the MKE and EKE, studies on multiscale ocean energetics should take special care. The RKE results from non-orthogonal separation of scales. Several scale-separation methods exist so far, each having different properties of RKE. This paper thoroughly introduces the scale-separation method recently sketched out by Zhou and Cheng (2021) — the PREM, and highlighted its advantages in the study of ocean kinetic energy balance. Conceptually, this method is an extension of the conventional REM method but applied to running windows of a predefined window length (or separation scale) across the observed time-record. Its two extreme scenarios, namely when window length equals record length or one, respectively reduce to the cases of REM and the universally employed RUM. The PREM, therefore, retains the nice features of both: it guarantees zero residual kinetic energy in the sense of time-mean which would otherwise be inevitable in RUM; it also enables varying background flow which is impossible in REM. Albeit PREM is only capable of representing the mean energies over a certain period around each time step, which is a drawback compared to instantly strict orthogonal methods like the localized multiscale window transform (Liang, 2012, 2016), it is still a handy tool thanks to the very simple mathematical formulae and the lightweight computational load.

In the study of mesoscale eddy energetics, another category of methods is especially useful: EDEX. Both PREM and RUM (i.e., the filtering methods) separate oceanic processes according to their timescale instead of their physical nature, whereas EDEX solely extracts mesoscale rotating eddies without screening on their duration. Mesoscale eddies are known as the dominant process on weekly to seasonal timescales depending on location and latitude. If the window length of PREM and RUM is chosen to match the timescale of mesoscale eddies in a particular area (large or small), then the separated "eddy-flow" is expected to include the mesoscale eddies and is thus comparable with the EDEX. However, since the window length is fixed but timescale of mesoscale eddies is not, the filtering methods would attribute non-eddy perturbations to the eddy-flow, and miss the longer-lived mesoscale eddies than the window length. Further, different physical processes on similar timescales as mesoscale eddies are distinguishable by EDEX but not by PREM and RUM. These are the advantages of EDEX in case the research interest is purely on mesoscale eddies, otherwise the filtering methods are more favorable when all perturbations defined by a given timescale is under study.

Realistic assessment and comparison of the PREM, RUM, and EDEX methods are presented in Section 5 in terms of the EKE, MKE, RKE, and the BTR, using satellite altimeter observations. For PREM and RUM, the window length is chosen to be one year, thus defining the "eddy-flow" as intra-annual variations. Results show that PREM and RUM give vastly different energy terms, with RUM severely underestimating mean intra-annual EKE and its interannual variability. Phase mismatch also exists between the two methods (min correlation = 0.38). The difference of EKE is the most prominent in strong current and eddy-active regions (max: Kuroshio Extension, RMSD = 60.3 J/m^3), but accounts for the largest fraction in areas with weak current and eddy (max: south of the Aleutian Islands, 208%). For a direct quantitative comparison of EKE in PREM and RUM please refer to Table 2 and Fig. 7. The mean mesoscale EKE and standard deviation from the EDEX method mostly resemble the intra-annual EKE of PREM especially in eddy-rich regions.

Based on the above results, it is proposed that in ocean multiscale energetic studies the scale-separation method should be carefully chosen. The PREM method is particularly useful if instantaneous energy budget is not required, while the EDEX could also provide better insight in case of pure mesoscale rotating eddies. However, the quantitative assessment presented in this work is only for intra-annual perturbations extracted by the 1-

Table 2. Comparison between EKE estimated by the PREM and RUM methods in various regions shown in Fig. 7

Region	MEAN		STD		RMSD		MIN CORR
	ABS	REL	ABS	REL	ABS	REL	
SPNP	1.38	0.44	1.63	1.81	2.47	2.08	0.38
KE	33.13	0.33	36.7	1.08	60.30	1.54	0.66
EWP	7.26	0.25	13.36	1.59	17.57	1.90	0.52
ESI	3.92	0.17	5.80	0.90	8.01	1.18	0.73
GS	17.69	0.16	17.35	0.49	33.52	0.87	0.69
SPNA	2.53	0.30	2.88	0.67	4.70	1.09	0.55
SPSA	1.51	0.33	2.17	1.08	3.23	1.55	0.62
ARC	16.93	0.15	16.59	0.55	29.82	0.90	0.73
BC	7.38	0.12	6.36	0.42	16.94	1.19	0.47
EA	6.46	0.05	7.49	0.19	15.74	0.49	0.85
SC	5.49	0.06	4.79	0.26	16.34	0.54	0.84
SPSP	3.56	0.26	3.58	0.61	6.42	0.88	0.73

Note: The compared quantities include: difference of time-mean EKE (MEAN), difference of interannual standard deviation (STD), and root-mean-square difference (RMSD), each of these are presented in terms of the absolute difference (ABS) in J/m^3, and the relative difference (REL). MEAN REL is relative to the mean EKE of RUM. STD REL and RMSD REL are relative to the standard deviation of RUM. The numbers are the maximum values in each region. The last column shows the minimal correlation coefficient (MIN CORR) between PREM and RUM EKEs. SPNP: subpolar North Pacific; KE: Kuroshio Extension; EWP: equatorial West Pacific; ESI: equatorial South Indian; GS: Gulf Stream; SPNA: subpolar North Atlantic; SPSA: subpolar South Atlantic; ARC: Agulhas Return Current; BC: Brazil Current; EA: East Australia; SC: Somali Current; SPSP: subpolar South Pacific.

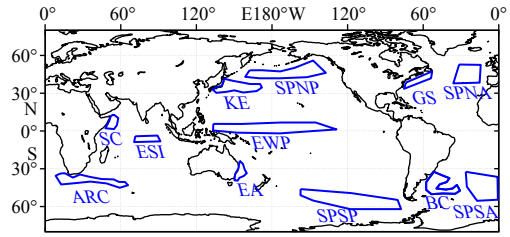

Fig. 7. Regions used in Table 2.

year window length, which may not be suitable for physical processes on other timescales. The current analysis is also limited to the sea surface kinetic energy and barotropic conversion, which is not adequate for a full picture of 3-D energy balance consisting also of the potential energy and baroclinic conversion. Restricted by satellite altimeter observations, this work only focuses on geostrophic velocity. For unbalanced flow on the submesoscale or smaller, the findings of this work might not hold. The present study should therefore be regarded as a prototype showcasing the features of the PREM and EDEX methods. Given the significant response of ocean eddies to climate change and their role in marine ecosystems, more precise evaluation of the EKE using the new methods is beneficial to the broader field of oceanography.

References

Akuetevi C Q C, Barnier B, Verron J, et al. 2016. Interactions between the Somali Current eddies during the summer monsoon: Insights from a numerical study. Ocean Science, 12(1): 185–205, doi: 10.5194/os-12-185-2016

Beal L M, Donohue K A. 2013. The Great Whirl: Observations of its seasonal development and interannual variability. Journal of Geophysical Research: Oceans, 118(1): 1–13, doi: 10.1029/2012JC008198

Bonaduce A, Cipollone A, Johannessen J A, et al. 2021. Ocean mesoscale variability: a case study on the mediterranean sea from a re-analysis perspective. Frontiers in Earth Science, 9: 724879, doi: 10.3389/feart.2021.724879

Bower A S, Armi L, Ambar I. 1995. Direct evidence of meddy formation off the southwestern coast of Portugal. Deep-Sea Research Part Ⅰ: Oceanographic Research Papers, 42(9): 1621–1630, doi: 10.1016/0967-0637(95)00045-8

Bower A S, Armi L, Ambar I. 1997. Lagrangian observations of meddy formation during a mediterranean undercurrent seeding experiment. Journal of Physical Oceanography, 27(12): 2545–2575, doi: 10.1175/1520-0485(1997)027<2545:LOOMFD>2.0.CO;2

Chen Ru, Flierl G R, Wunsch C. 2014. A description of local and nonlocal eddy–mean flow interaction in a global eddy-permitting state estimate. Journal of Physical Oceanography, 44(9): 2336–2352, doi: 10.1175/JPO-D-14-0009.1

Chen Xiao, Qiu Bu, Chen Shuiming, et al. 2015. Seasonal eddy kinetic energy modulations along the North Equatorial Countercurrent in the western Pacific. Journal of Geophysical Research: Oceans, 120(9): 6351–6362, doi: 10.1002/2015JC011054

Chen Ru, Thompson A F, Flierl G R. 2016. Time-dependent eddy-mean energy diagrams and their application to the ocean. Journal of Physical Oceanography, 46: 2827–2850, doi: 10.1175/JPO-D-16-0012.1

Cheng Yu-Hsin, Ho Chung-Ru, Zheng Quanan, et al. 2014. Statistical characteristics of mesoscale eddies in the North Pacific derived from satellite altimetry. Remote Sensing, 6(6): 5164–5183, doi: 10.3390/rs6065164

Cheng Xuhua, McCreary J P, Qiu Bo, et al. 2018. Dynamics of eddy generation in the central Bay of Bengal. Journal of Geophysical Research: Oceans, 123(9): 6861–6875, doi: 10.1029/2018JC014100

Clarke A J. 1983. The reflection of equatorial waves from oceanic boundaries. Journal of Physical Oceanography, 13(7): 1193–1207, doi: 10.1175/1520-0485(1983)013<1193:TROEWF>2.0.CO;2

Di Lorenzo E, Foreman M G G, Crawford W R. 2005. Modelling the generation of Haida Eddies. Deep-Sea Research Part II: Topical Studies in Oceanography, 52(7–8): 853–873, doi: 10.1016/j.dsr2.2005.02.007

Drillet Y, Bourdallé-Badie R, Siefridt L, et al. 2005. Meddies in the Mercator North Atlantic and Mediterranean Sea eddy-resolving model. Journal of Geophysical Research: Oceans, 110(C3): C03016, doi: 10.1029/2003JC002170

Ducet N, Le Traon P Y, Reverdin G. 2000. Global high-resolution mapping of ocean circulation from TOPEX/Poseidon and ERS-1 and -2. Journal of Geophysical Research: Oceans, 105(C8): 19477–19498, doi: 10.1029/2000JC900063

Faghmous J H, Frenger I, Yao Yuanshun, et al. 2015. A daily global mesoscale ocean eddy dataset from satellite altimetry. Scientific Data, 2: 150028, doi: 10.1038/sdata.2015.28

Fu L L, Qiu Bo. 2002. Low-frequency variability of the North Pacific Ocean: the roles of boundary- and wind-driven baroclinic Rossby waves. Journal of Geophysical Research: Oceans, 107(C12): 13-1–13-10, doi: 10.1029/2001JC001131

Jia Fan, Wu Lixin, Qiu Bo. 2011. Seasonal modulation of eddy kinetic energy and its formation mechanism in the southeast Indian Ocean. Journal of Physical Oceanography, 41(4): 657–665, doi: 10.1175/2010JPO4436.1

Jouanno J, Sheinbaum J, Barnier B, et al. 2012. Seasonal and interannual modulation of the eddy kinetic energy in the Caribbean Sea. Journal of Physical Oceanography, 42(11): 2041–2055, doi: 10.1175/JPO-D-12-048.1

Kang Dujuan, Curchitser E N. 2015. Energetics of eddy–mean flow interactions in the Gulf Stream region. Journal of Physical Oceanography, 45(4): 1103–1120, doi: 10.1175/JPO-D-14-0200.1

Kang Dujuan, Curchitser E N. 2017. On the evaluation of seasonal variability of the ocean kinetic energy. Journal of Physical Oceanography, 47(7): 1675–1683, doi: 10.1175/JPO-D-17-0063.1

Liang X S. 2012. Multiscale window interaction and localized nonlinear hydrodynamic stability analysis. In: Oh H W, ed. Advanced Fluid Dynamics. IntechOpen, 159–182, https://www.intechopen.com/books/1013 [2012–03–09/2024–01–29]

Liang X S. 2016. Canonical transfer and multiscale energetics for primitive and quasigeostrophic atmospheres. Journal of the Atmospheric Sciences, 73(11): 4439–4468, doi: 10.1175/JAS-D-16-0131.1

Liu W T, Xie Xiaosu, Niiler P P. 2007. Ocean–atmosphere interaction over agulhas extension meanders. Journal of Climate, 20(23): 5784–5797, doi: 10.1175/2007JCLI1732.1

Paillet J, Le Cann B, Carton X, et al. 2002. Dynamics and evolution of a northern meddy. Journal of Physical Oceanography, 32(1): 55–79, doi: 10.1175/1520-0485(2002)032<0055:DAEOAN>2.0.CO;2

Penduff T, Barnier B, Dewar W K, et al. 2004. Dynamical response of the oceanic eddy field to the North Atlantic Oscillation: a model–data comparison. Journal of Physical Oceanography, 34(12): 2615–2629, doi: 10.1175/JPO2618.1

Pope S B. 2000. Turbulent Flows. New York, NY, USA: Cambridge University Press

Qiu Bo, Chen Shuiming. 2010. Eddy-mean flow interaction in the decadally modulating Kuroshio Extension system. Deep-Sea Research Part Ⅱ: Topical Studies in Oceanography, 57(13/14): 1098–1110, doi: 10.1016/j.dsr2.2008.11.036

Qiu Bo, Chen Shuiming, Schneider N, et al. 2014. A coupled decadal prediction of the dynamic state of the Kuroshio Extension system. Journal of Climate, 27(4): 1751–1764, doi: 10.1175/JCLI-D-13-00318.1

Reynolds O. 1895. On the dynamical theory of incompressible viscous fluids and the determination of the criterion. Philosophical Transactions of the Royal Society A: Mathematical, Physical and Gineering sciences, 186: 123–164, doi: 10.1098/rsta.1895.0004

Rogachev K A, Shlyk N V. 2018. The role of the aleutian eddies in the

Kamchatka Current warming. Russian Meteorology and Hydrology, 43(1): 43–48, doi: 10.3103/S1068373918010065
Rogachev K A, Shlyk N V. 2019. Characteristics of the Kamchatka Current eddies. Russian Meteorology and Hydrology, 44(6): 416–423, doi: 10.3103/S1068373919060062
Rogachev K, Shlyk N, Carmack E. 2007. The shedding of mesoscale anticyclonic eddies from the Alaskan Stream and westward transport of warm water. Deep-Sea Research Part Ⅱ: Topical Studies in Oceanography, 54(23–26): 2643–2656, doi: 10.1016/j.dsr2.2007.08.017
Saito R, Yamaguchi A, Yasuda I, et al. 2014. Influences of mesoscale anticyclonic eddies on the zooplankton community south of the western Aleutian Islands during the summer of 2010. Journal of Plankton Research, 36(1): 117–128, doi: 10.1093/plankt/fbt087
Seo H. 2017. Distinct influence of air-sea interactions mediated by mesoscale sea surface temperature and surface current in the Arabian Sea. Journal of Climate, 30(20): 8061–8080, doi: 10.1175/JCLI-D-16-0834.1
Serra N, Ambar I. 2002. Eddy generation in the Mediterranean undercurrent. Deep-Sea Research Part Ⅱ: Topical Studies in Oceanography, 49(19): 4225–4243, doi: 10.1016/S0967-0645(02)00152-2
Serra N, Ambar I, Käse R H. 2005. Observations and numerical modelling of the Mediterranean outflow splitting and eddy generation. Deep-Sea Research Part Ⅱ: Topical Studies in Oceanography, 52(3/4): 383–408, doi: 10.1016/j.dsr2.2004.05.025
Trott C B, Subrahmanyam B, Murty V S N. 2017. Variability of the Somali Current and eddies during the southwest monsoon regimes. Dynamics of Atmospheres and Oceans, 79: 43–55, doi: 10.1016/j.dynatmoce.2017.07.002
von Storch J S, Eden C, Fast I, et al. 2012. An estimate of the Lorenz energy cycle for the World Ocean based on the 1/10° STORM/NCEP simulation. Journal of Physical Oceanography, 42(12): 2185–2205, doi: 10.1175/JPO-D-12-079.1
Wang Lei, Yu Jinyi. 2018. A recent shift in the monsoon centers associated with the tropospheric biennial oscillation. Journal of Climate, 31(1): 325–340, doi: 10.1175/JCLI-D-17-0349.1
Wang Sen, Zhu Weijun, Ma Jing, et al. 2019. Variability of the Great Whirl and its impacts on atmospheric processes. Remote Sensing, 11(3): 322, doi: 10.3390/rs11030322
Yang Yang, Liang X S. 2016. The instabilities and multiscale energetics underlying the mean–interannual–eddy interactions in the Kuroshio Extension region. Journal of Physical Oceanography, 46(5): 1477–1494, doi: 10.1175/JPO-D-15-0226.1
Yang Yang, Liang X S. 2019. Spatiotemporal variability of the global ocean internal processes inferred from satellite observations. Journal of Physical Oceanography, 49(8): 2147–2164, doi: 10.1175/JPO-D-18-0273.1
Zenk W, Schultz Tokos K, Boebel O. 1992. New observations of meddy movement south of the Tejo Plateau. Geophysical Research Letters, 19(24): 2389–2392, doi: 10.1029/92GL02139
Zhou Guidi, Cheng Xuhua. 2021. On the errors of estimating oceanic eddy kinetic energy. Journal of Geophysical Research: Oceans, 126(2): e2020JC016449, doi: 10.1029/2020JC016449
Zhou Guidi, Cheng Xuhua. 2022. Impacts of oceanic fronts and eddies in the Kuroshio-Oyashio Extension region on the atmospheric general circulation and storm track. Advances in Atmospheric Sciences, 39(1): 22–54, doi: 10.1007/s00376-021-0408-4
Zhou Guidi, Li Zhuhua, Cheng Xuhua. 2021a. Intrinsic and wind-driven decadal variability of the Kuroshio Extension in altimeter observations. Frontiers in Marine Science, 8: 766226, doi: 10.3389/fmars.2021.766226
Zhou Jiang, Zhou Guidi, Liu Hailong, et al. 2021b. Mesoscale eddy-induced ocean dynamic and thermodynamic anomalies in the North Pacific. Frontiers in Marine Science, 8: 756918, doi: 10.3389/fmars.2021.756918

Supplementary information:

Fig. S1. Fraction of the difference between 28-year averaged energy terms estimated by the PREM and RUM methods, relative to the energy terms of the RUM method. The terms are MKE (a) and EKE (b).

Fig. S2. Fraction of the interannual standard deviation of the energy terms estimated by the PREM method, relative to the 28-year average (left column) and fraction of difference of interannual standard deviation of the energy terms estimated by the PREM and RUM methods, relative to the standard deviation of the RUM method (right column). The energy terms are MKE (top row), and EKE (bottom row).

Fig. S3. Twenty-eight-year averaged energy terms estimated by the EDEX-B method (top row), interannual standard deviation of the energy terms of the EDEX-B method (bottom row), and correlation of the energy terms of the EDEX-B and PREM methods (middle row). The energy terms are MKE (left column), and EKE (right column).

Fig. S4. The ratio of 28-year averaged EKE (a) and interannual standard deviation of EKE (b) estimated by the EDEX-B method relative to the EDEX, shown in logarithmic scale.

The supplementary information is available online at https://doi.org/10.1007/s13131-024-2365-0 and http://www.aosocean.com/. The supplementary information is published as submitted, without typesetting or editing. The responsibility for scientific accuracy and content remains entirely with the authors.